Effect of temperature on fast hydrogen diffusion in iron: A path-integral quantum dynamics approach

Hajime Kimizuka,* Hideki Mori, and Shigenobu Ogata

Department of Mechanical Science and Bioengineering, Graduate School of Engineering Science, Osaka University, Osaka 560-8531, Japan

(Received 17 December 2010; published 8 March 2011)

Here we explicitly present the diffusion coefficients (D) and activation energies (E_a) of interstitial H in α-Fe over a temperature range of 100 to 1000 K. These values were predicted by applying path-integral molecular dynamics modeling based on first principles. The obtained D and E_a values exhibit clear non-Arrhenius temperature dependence and a transition from quantum to classical behavior at around 500 K. Our results show that the quantum effects not only significantly lower the diffusion barrier but also change the diffusion pathway even at room temperature; thus, fast diffusion becomes possible.

DOI: 10.1103/PhysRevB.83.094110 PACS number(s): 66.30.jp, 02.70.Ns

I. INTRODUCTION

The behavior of H in materials has received much attention for a number of technological applications, including the use of H gas as a secondary energy carrier, H gas storage and purification, and fusion reactor technology.[1,2] In particular, H diffusion in Fe and Fe alloys is considerably important because it leads to engineering problems caused by H embrittlement and degradation of high-strength steels, reactor materials, etc. The diffusion coefficients of H in α-Fe are the highest among the values reported thus far for any metal.[3] Detailed information on the behavior of H in Fe is important for understanding the elementary processes of such fast solid-state diffusion and transport in Fe-H systems. This high H diffusivity is believed to result from the very low activation energies due to the quantum nature of H. However, because of the lack of experimental observations and results obtained by modeling and simulation, the details on the mechanism of H diffusivity have not yet been established.

While a large number of experimental studies have been conducted on H diffusion (for reviews see Refs. 3–5), there is very little reliable data available, particularly on diffusion at temperatures below room temperature. Several reasons for the poor agreement between different measurements have been proposed: surface barrier effects, trapping of H by impurities, dislocations, grain boundaries, or precipitates, and the formation of molecular H in micropores.[4,5] Owing to the low solubility of H in Fe, experiments have to be performed at low H concentrations ($<$1 ppm under ambient conditions); therefore, the experiments are extremely sensitive to trapping effects. Thus, even in the case of pure Fe, the experimental information on H diffusivity is unreliable compared to that on H diffusion in other bcc metals (V, Nb, Ta, etc.).

First-principles calculations and approaches based on classical molecular mechanics have been used to study the H adsorption, absorption, dissolution, and diffusion energetics in the case of body-centered cubic (bcc) Fe in several studies.[6–11] Modern *ab initio* modeling is expected to provide a good description of the geometries, energetics, and potential energy surface in Fe-H systems. However, to our knowledge, there is no systematic derivation of the diffusion coefficients and activation energies in which quantum effects over a wide temperature range have been considered. Such a derivation is essential for understanding the possible mechanisms of H diffusion in Fe.

We report the diffusion coefficients (D) and corresponding activation energies (E_a) of interstitial H in α-Fe at various temperatures, as determined by using the path-integral (PI) molecular dynamics method along with a newly developed *ab initio*–based potential; in our calculations, we took quantum effects into consideration. Our main objective is to present results of the PI calculations that can be performed to quantitatively evaluate the H diffusivity in α-Fe over a wide temperature range and to investigate the microscopic mechanism of local diffusion of H interstitials. The data thus obtained can be compared with experimental data.

II. METHODS

A. *Ab initio*–based analytical potential for the Fe-H system

For specific use in PI simulations, an interatomic potential for the Fe-H system was constructed within the embedded-atom-method (EAM) formalism.[12] The energy of a system is defined in accordance with the EAM scheme:

$$E = \frac{1}{2}\sum_{j\neq i}^{N}\phi_{ij}(r_{ij}) + \sum_{i}^{N}F_i(\bar{\rho}_i), \tag{1}$$

where r_{ij} is the distance between atoms i and j, and ϕ_{ij} is the two-body part of the potential between atoms i and j. F_i is the embedding energy and $\bar{\rho}_i$ is the electron density at atom i due to the remaining atoms in the system. The density $\bar{\rho}_i$ is defined as

$$\bar{\rho}_i = \sum_{j\neq i}^{N}\rho_j(r_{ij}), \tag{2}$$

where ρ_j is the electron density contributed by atom j. The present potential for the Fe-H system consists of seven functions: ϕ_{FeFe}, ϕ_{HH}, ϕ_{FeH}, F_{Fe}, F_{H}, ρ_{Fe}, and ρ_{H}. In this model, interactions between pure elements are represented by existing EAM potentials. The form of ϕ_{FeFe}, F_{Fe}, and ρ_{Fe} for Fe is predetermined on the basis of the studies conducted by Mendelev *et al.*[13,14] For the functions ϕ_{HH}, F_{H}, and ρ_{H}, we used the model developed by Angelo *et al.*,[15] in which the parameters were corrected by Baskes *et al.*[16]

The remaining pair interaction ϕ_{FeH} is described by the Morse function as

$$\phi_{\mathrm{FeH}}(r) = \alpha_1[e^{-2\alpha_2(r-\alpha_3)} - 2e^{-\alpha_2(r-\alpha_3)}], \tag{3}$$

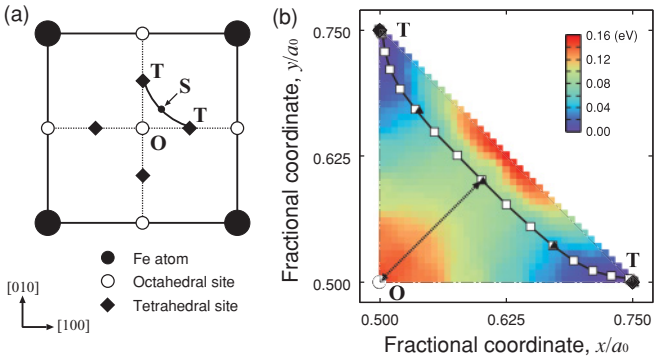

FIG. 1. (Color online) (a) Positions of T-sites and O-sites. (b) MEP on the (001) plane of the bcc-Fe lattice. The S-site is the saddle point along the MEP (open squares) for direct hopping of a H atom between two neighboring T-sites. The DFT-based MEP (triangles) has been taken from Ref. 7.

where α_1, α_2, and α_3 are fitting parameters. A linear term is added to ϕ_{FeH} to provide a smooth cutoff at the cutoff distance r_c. This term is given by

$$\phi(r) = \phi_{\mathrm{FeH}} + a(r - r_c) + b, \tag{4}$$

where $a = -\phi'_{\mathrm{FeH}}(r_c)$ and $b = -\phi_{\mathrm{FeH}}(r_c)$. To develop the EAM potential for the Fe-H system, F_{H} is modified so that the total H energy is not affected. The form of the modification is

$$\rho_{\mathrm{H}} = S_{\mathrm{H}}\rho_{\mathrm{H}}, \tag{5}$$

$$F_{\mathrm{H}}(\bar{\rho}) = F_{\mathrm{H}}(\bar{\rho}/S_{\mathrm{H}}), \tag{6}$$

where S_{H} is the relative scaling factor for ρ_{H}.

In this study, the parameters S_{H} and α_i are fitted to reproduce the activation barrier at the transition state for H migration in α-Fe, whose energies and geometries have been obtained from the spin-polarized density functional theory (DFT) calculations presented in the literature.[7] The minimum energy path (MEP) and the transition state between two adjacent tetrahedral sites (T-sites) for the EAM potential are identified by using the nudged elastic band (NEB) method[17] with an $Fe_{128}H$ supercell ($4 \times 4 \times 4$ unit cells). As shown in Fig. 1, the S-site, which is the saddle point for the relaxed potential energy surface, is located in the vicinity of the midpoint between the two neighboring T-sites, at a distance δ_S from the octahedral site (O-site). The parameters are then optimized to represent the migration energy (the energy barrier along the MEP) E_m, the distance between the O-site and S-site δ_S, and the difference between the energies of the H atom at the O-site and the T-site $E_{\mathrm{T-O}}$. The zero-point energy (ZPE) contributions are excluded while calculating these energy values.[7] Therefore, the present analytic potential model describes the *ab initio*–based "bare" (not ZPE-corrected) potential energy surface for the Fe-H system. The obtained parameters for ϕ_{FeH} are listed in Table I.

Table II lists the calculated values of E_m, δ_S, $E_{\mathrm{T-O}}$, the dissolution energy at the T-site (E_s), and the increase in the volume of the relaxed $Fe_{128}H$ cell with respect to the volume of the relaxed Fe_{128} cell (ΔV). The results for the potential developed by Wen *et al.*[9] are also listed. Our potential is confirmed to reproduce the DFT energy differences among the T-site, S-site, and O-site, where a H atom may reside, as well as the DFT-based MEP (Fig. 1). We apply our model of Fe-H potential to the following PI analysis.

TABLE I. Parameters for the mixed two-body potential ϕ_{FeH}.

Parameter	ϕ_{FeH}
S_{H}	32.0
α_1 (eV)	0.0968
α_2 (Å^{-1})	4.33
α_3 (Å)	1.65
a (10^{-5} eV/Å)	−1.34315
b (10^{-6} eV)	3.10198
r_c (Å)	4.2

Here, it is noted that the DFT calculations in the literature[7] provided almost the same energy differences between the O-site and T-site for different concentrations of Fe/H = 16, 54, and 128. In the case of H in the regular Fe lattice, an extremely concentrated state, such as Fe/H < 16, is unlikely to occur in the ordinary conditions owing to the positive enthalpy of solution and very low solubility of H in Fe. Thus we assume that many-body interactions between H atoms do not dominate the diffusion behavior of H, and the energy landscape described by this potential reflects a reasonable situation.

B. Centroid path-integral molecular dynamics calculations

To investigate the real-time quantum dynamics of H in Fe, a semiclassical method called centroid path-integral molecular dynamics (CMD)[18,19] was employed. Here, the centroids of the isomorphic Feynman beads[20] of a quantum particle evolve in real time according to the statistical mean force. The system consists of cyclic chains of beads (P beads on each chain) coupled by harmonic springs, as shown in Fig. 2. The spring constant of the chains is $m_i P/(\beta\hbar)^2$. Here, m_i represents the mass of the ith quantum particle; β, the inverse temperature $(k_B T)^{-1}$; k_B, the Boltzmann constant; and $\hbar$, the Planck constant. The isomorphism becomes exact in the limit $P \to \infty$.

In the CMD method, centroid trajectories of a quantum particle are generated by the semiclassical equation of motion

$$m_I \ddot{\boldsymbol{R}}_I(t) = \langle \boldsymbol{F}_I(\boldsymbol{R}_1, \cdots, \boldsymbol{R}_N)\rangle_{\mathrm{PI}} \qquad (I = 1, \ldots, N), \tag{7}$$

where $\boldsymbol{R}_I(t)$ represents the centroid position of the Ith particle in the physical system. The right-hand side of Eq. (7) is the

TABLE II. Calculated values of the migration energy (E_m), distance between the O-site and S-site (δ_S), the difference between the energies of the H atom ($E_{\mathrm{T-O}} = E_{\mathrm{O}} - E_{\mathrm{T}}$) at the O-site and T-site, dissolution energy (E_s) of H at the T-site, and percentage change in volume (ΔV). The target DFT energies in the literature[7] are not ZPE-corrected values.

	DFT[a]	Our Model	Wen
E_m (eV)	0.088	0.088	0.029
δ_S (Å)	0.407	0.407	0.217
$E_{\mathrm{T-O}}$ (eV)	0.13	0.144	0.035
E_s (eV)	0.20	0.201	0.29
ΔV (%)	0.06	0.108	0.21

[a]Reference 7.

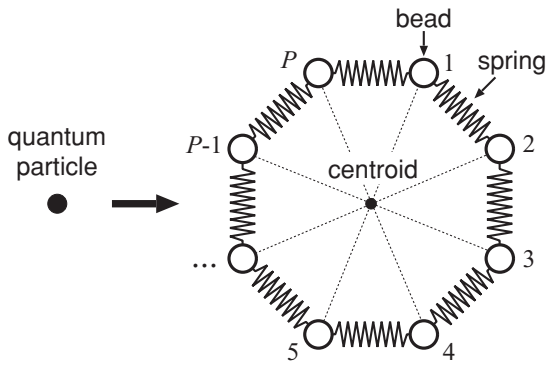

FIG. 2. Schematic illustration of a discretized P-point ("bead") cyclic path for a single quantum particle.

path-integral average of the centroid force

$$\boldsymbol{F}_I\left(\boldsymbol{R}_1^C,\ldots,\boldsymbol{R}_N^C\right)=\sum_{s=1}^{P}\boldsymbol{f}_I^{(s)}=-\frac{1}{P}\sum_{s=1}^{P}\frac{\partial\Phi\left(\{\boldsymbol{r}_i^{(s)}\}\right)}{\partial\boldsymbol{r}_I^{(s)}},\qquad(8)$$

where $\boldsymbol{r}_i^{(s)}$ is the position of the sth bead of the ith particle, $\boldsymbol{f}_I^{(s)}$ is the force acting on each bead, and $\boldsymbol{R}_i^C$ is the centroid variable, which is the center of mass of P beads of the ith particle, $\boldsymbol{R}_i^C=(1/P)\sum_{s=1}^{P}\boldsymbol{r}_i^{(s)}$. The potential of the isomorphic beads is given as

$$V\left(\{\boldsymbol{r}_i^{(s)}\}\right)=\sum_{i=1}^{N}\sum_{s=1}^{P}\left[\frac{1}{2}k_i\left(\boldsymbol{r}_i^{(s)}-\boldsymbol{r}_i^{(s+1)}\right)^2+\frac{1}{P}\Phi\left(\{\boldsymbol{r}_i^{(s)}\}\right)\right],\qquad(9)$$

where Φ is the physical potential, k_i is the spring constant between the neighboring beads $k_i=m_iP/(\beta\hbar)^2$, and $\boldsymbol{r}_i^{(P+1)}=\boldsymbol{r}_i^{(1)}$. To uncouple the harmonic bead-bead interaction term in Eq. (9), the bead coordinates $\{\boldsymbol{r}_i^{(s)}\}$ are transformed to normal-mode coordinates.[18,19]

Real-time evolutions of the mean square displacements (MSDs) of the centroids of H atoms in α-Fe are determined at various temperatures. Generally, seven temperatures are chosen: $T=100$, 200, 300, 400, 500, 750, and 1000 K. To carry out the CMD calculations, massive Nosé-Hoover chains[23] are attached to normal-mode coordinates,[18,19] while a single Nosé-Hoover thermostat[21,22] is attached to the centroid coordinates. We consider the $Fe_{128}H$ supercell under periodic boundary conditions and initially place a H atom at one of the T-sites in a bcc-Fe structure with lattice length $a_0=2.8553$ Å. In order to characterize the quantum effects on the H diffusion, the CMD results are compared to those obtained by classical molecular dynamics (MD) calculations based on our potential or that of Wen *et al.* In both CMD and classical MD calculations, the integration time step is $\Delta\tau=0.1$ fs. In the CMD calculations, the multiple time step method based on the reference system propagator algorithm (RESPA)[24] is employed for time integration; the normal-mode coordinates and centroid coordinates are integrated at intervals of $0.1\,\Delta\tau$ and $\Delta\tau$, respectively. The centroids evolve with time according to an instantaneous force; the evolution is based on an on-the-fly scheme.[18,19] In this analysis, all atoms are treated quantum-mechanically by discretizing the path into $P=64$ imaginary-time slices.

The diffusion coefficients at each temperature are evaluated using Einstein's relation from the MSDs within the canonical ensemble for a 0.3-ns run. In the CMD approach, dynamical rearrangements of Fe atoms during the H-diffusion process are automatically taken into account. Thus the obtained results include the phonon effects on H diffusion in the Fe lattice. In our model, the Fe lattice is assumed to maintain the bcc structure over a target temperature range of 100–1000 K, which is below the transition temperature between bcc α-Fe and fcc γ-Fe (ca. 1179 K) and also the Curie point (ca. 1043 K).[3] We should note that the spin fluctuation effects are not included in the analysis.

III. RESULTS AND DISCUSSION

A. Diffusion coefficients

Figure 3 shows the Arrhenius plots of the diffusion coefficients of H in α-Fe. The coefficients were obtained by the CMD and classical MD methods. In the classical MD results, the logarithmic D value varies linearly with the reciprocal temperature. Thus, in the classical regime, a thermally activated process controls the rate over the entire temperature range, namely, 100–1000 K. In contrast, for our potential, a strong bending is observed at around 500 K in the Arrhenius plots based on the CMD results and a deviation from the linear behavior with decreasing temperature is also observed, while the CMD and classical MD results agree with each other at high temperatures. This indicates that the *apparent* activation energy for H diffusion decreased because of the quantum tunneling at low temperatures. Note that such a non-Arrhenius diffusivity of H in Fe has not been clearly observed in experiments, although similar behavior is observed in group-V bcc transition metals such as Nb and Ta (however, the bending in this case is observed *below* room temperature).[3,4]

For comparison, the experimental D values from Refs. 25–30 are also plotted in Fig. 3. In general, the scatter of the measured D values of H in Fe in the literature even reaches three or four orders of magnitude particularly at room temperature,[3–5] depending on the purity of the specimen. We chose the D values[25–30] on the basis that the experiments were performed with specimens of well-annealed or zone-refined high purity Fe, in order to avoid the trapping effects on measured H diffusivities. In Fig. 3, our CMD results are in reasonable agreement with the experimental measurements over a wide temperature range (300–1000 K). Also, the calculated and experimental D values[26–28] at 300 K and 1000 K are given in Table III. We confirm that the present CMD approach is valid

TABLE III. Calculated values for diffusion coefficients (D in 10^{-8} m^2 s^{-1}) of H in α-Fe, together with experimental values.

	$T=300$ K	$T=1000$ K
Calc. (Classical MD)	0.29	2.39
Calc. (CMD)	0.83	2.37
Expt. (Ref. 28)	0.87[a]	2.63[b]
Expt. (Refs. 26,27)	0.74[a]	2.45[b]

[a]At 293 K.
[b]At 973 K.

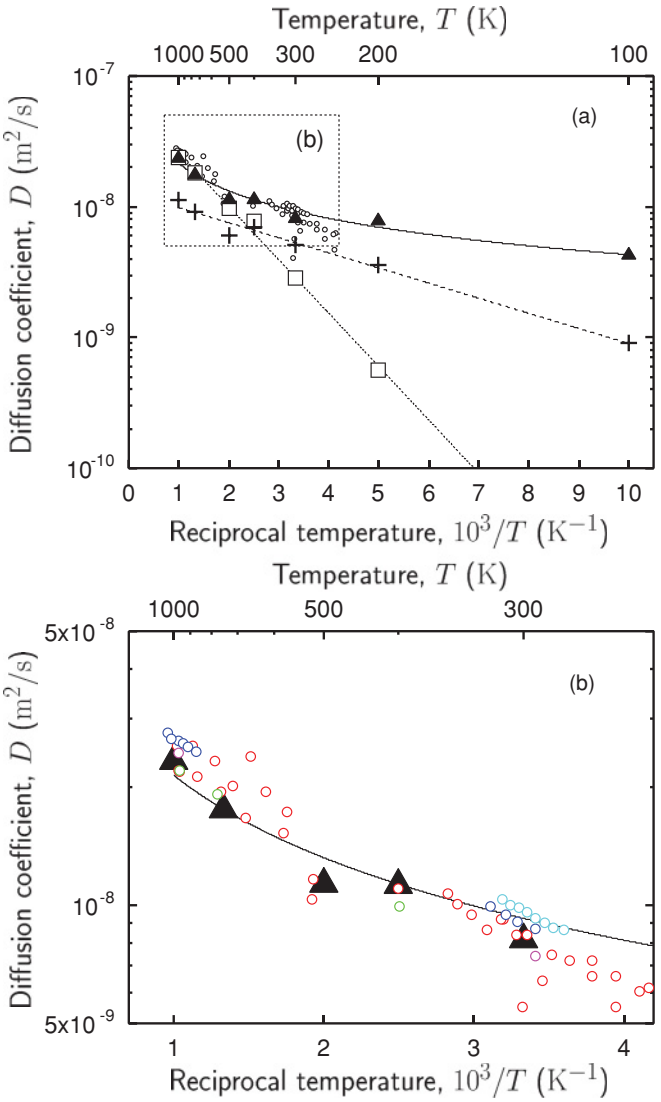

FIG. 3. (Color online) Diffusion coefficients of H in Fe in the temperature range 100–1000 K. The solid triangles and open squares represent the CMD and classical MD results for our potential, respectively. The experimental data (open circles) have been taken from Refs. 25–30. The cross symbols represent the classical MD results for the potential of Wen *et al.*

for predicting the absolute values of the diffusion coefficients both below and above the temperature of 500 K.

In several experimental studies, the E_a values were practically estimated by the slope of the $\ln D$ versus $1/T$ plot between ca. 300 K and 1000 K,[27–29] as listed in Table IV. To compare with these results, we evaluate the slope and intercept of the CMD-based D values by linear approximation over the temperature range 300–1000 K; the obtained E_a value of 0.037 eV shows good agreement with the experimental data in the range of 0.035–0.044 eV.[27–29] Also, the CMD values of the preexponential factor (D_0) agree well with the experimental data.[27–29] Since the classical limit of the migration barrier E_m on the present potential energy surface is set to 0.088 eV, the apparent E_a is confirmed to decrease by 58% when quantum effects are considered. It is found that the H diffusivity in the quantum regime is much higher than that in the classical one,

TABLE IV. Calculated values for an activation energy (E_a) and a preexponential factor (D_0) of H diffusivity in α-Fe in the temperature range of 300–1000 K, together with experimental values.

	E_a (eV)	D_0 (10^{-8} m^2 s^{-1})
Calc. (Classical MD)	0.081	5.92
Calc. (CMD)	0.037	3.23
Expt.[a] (Ref. 29)	0.035	3.35
Expt.[b] (Ref. 28)	0.040	4.20
Expt.[c] (Ref. 27)	0.044	4.15

[a]Between 240 and 970 K.
[b]Between 290 and 1040 K.
[c]Obtained only at two temperatures: 293 and 973 K.

and it strongly deviates from that in a pure thermally activated regime at temperatures below 500 K. This indicates that the H diffusivity in Fe exhibits the transition from classical to quantum behavior with decreasing temperature.

On the other hand, in the classical MD result for the potential of Wen *et al.*, the value of $E_a = 0.023$ eV is closer to the experimental values than the value in the classical MD result for our potential (0.081 eV) because their potential was fit to the measured experimental data, which include ZPE contributions. However, the D values deviate significantly from the experimental values, as shown in Fig. 3. Naturally, quantum tunneling effects are not considered in the classical MD approach, and this approach cannot be adopted to describe a nonlinear temperature dependence of the H diffusivity associated with a change in the diffusion mechanism, even when the interatomic potential is fit to the ZPE-corrected quantities.

B. Mechanism of local migration of H

To elucidate the mechanism of H migration in α-Fe, in real-time simulations, all possible trajectories of H centroids are folded into one unit cell. Figure 4 shows the obtained H density distribution on the square (001) plane surrounded by four T-sites, at temperatures below room temperature. The vibrational motion of H around the T-sites has a dominant influence on these results. This is reflected by the fact that the configuration with the lowest potential energy is the T-site. In the case of the classical MD results, the jumping of H atoms between adjacent T-sites dominates the diffusive motion; on the other hand, in the case of the CMD results, we confirm that H atoms can approach or even pass over the O-sites at lower temperatures. This indicates that the quantum effects strongly control the mechanism of local diffusion of H in α-Fe.

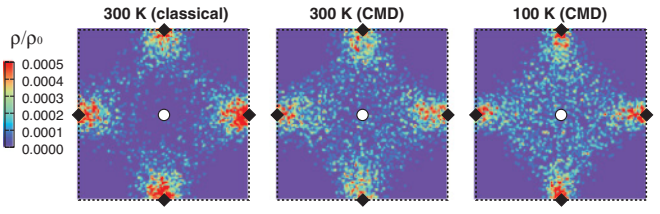

FIG. 4. (Color online) Positions of H atoms, as obtained from the classical MD and CMD calculations. The trajectories for the H atom are folded on the (001) plane of the bcc unit cell. The open circles and solid diamonds represent the O-sites and T-sites, respectively.

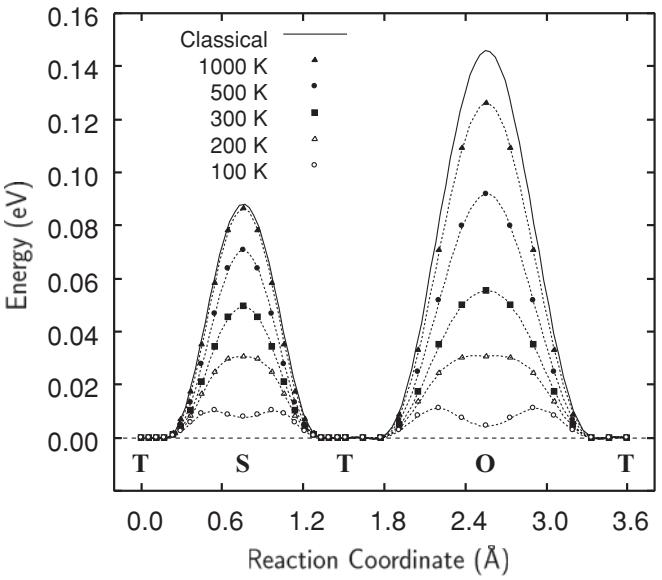

FIG. 5. Free energy profiles for H migration along the path between neighboring T-sites at various temperatures.

To characterize the change in the diffusion path and apparent activation energy with temperature, we evaluated the differences between the free energies of the system ΔF for H at the interstitial T-site, S-site, and O-site using the path-integral molecular dynamics (PIMD) method; the classical isomorph was simulated by a molecular dynamics method; then, the static averages (e.g., mean forces and spatial distributions) were calculated by sampling configurations of the system using the statistical weight. First, the MEP and the transition state for H diffusion in α-Fe were obtained by using the NEB method[17] in the classical regime. An interpolated chain of configurations (images) between the initial and final positions (i.e., neighboring T-sites) was connected by springs and simultaneously relaxed so that it becomes the MEP. Each of the obtained images along the MEP is supposed to correspond to the centroid configuration $\boldsymbol{\mathcal{R}} = \{\boldsymbol{R}_i\}$ of the quantum chains. Then, the mean force $\langle \boldsymbol{\mathcal{F}}(\boldsymbol{\mathcal{R}}) \rangle_{\mathrm{PI}}$ was calculated in the canonical ensemble with fixed centroid positions; here, $\boldsymbol{\mathcal{F}}(\boldsymbol{\mathcal{R}})$ is the force acting on the quantum chains when the centroids are located at $\boldsymbol{\mathcal{R}}$, and the quantities in brackets are path-integral average values. The ΔF was evaluated by integrating the mean force along the diffusion path $\boldsymbol{\mathcal{S}}$, i.e.,[31]

$$\Delta F = -\int d\boldsymbol{\mathcal{S}} \cdot \langle \boldsymbol{\mathcal{F}}(\boldsymbol{\mathcal{R}}) \rangle_{\mathrm{PI}}. \tag{10}$$

We calculated ΔF for H at five temperatures between 100 and 1000 K, along the path from a T-site to an S-site (T-S) and the line from the T-site to the O-site (T-O).

Figure 5 shows the PIMD-based free energy profiles for H migration at various temperatures. We can confirm that the migration energy of H in α-Fe dramatically decreases as temperature decreases, along both the T-S and T-O paths. The PIMD-based diffusion barrier of the T-S path at an ambient

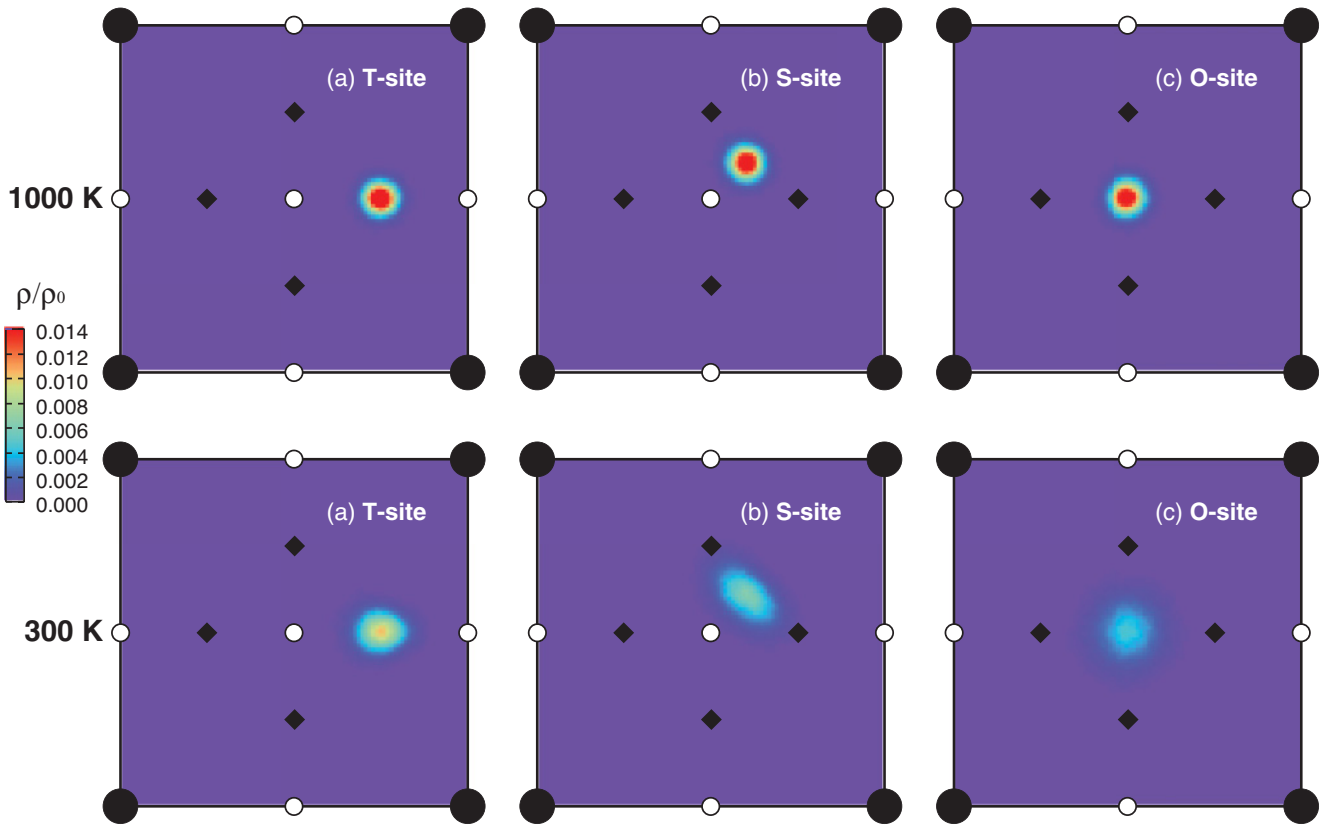

FIG. 6. (Color online) Quantum distribution of a H atom at different temperatures, i.e., at 1000 K and 300 K. At each temperature, the results are shown with the centroid of the H atom located at the (a) T-site, (b) S-site, and (c) O-site. The open circles, diamonds, and solid circles represent the O-sites, T-sites, and equilibrium positions of the Fe atoms, respectively.

temperature of 300 K is calculated as 0.049 eV, which agrees well with the ZPE-corrected DFT value of 0.042 eV reported by Jiang and Carter.[7] In particular, the T-O diffusion barrier is more sensitive to temperature than the T-S barrier; the T-O barrier at 300 K decreases by 61% relative to the classical limit, while the T-S barrier decreases by 43%. This suggests that the quantum tunneling effects become dominant at ambient temperatures and that not only the T-S but also the T-O diffusion paths become more accessible at lower temperatures.

To investigate the state of a H atom in Fe, three centroid positions were considered: a T-site, an S-site, and an O-site. Figure 6 shows the quantum distributions of a H atom at different temperatures. At a high temperature of 1000 K, the H-atom distribution at all sites is rather confined and isotropic on the (001) plane. On the other hand, at 300 K, the distribution at the S-site broadens substantially and is more spread out between the two T-sites. Further, the distribution at the O-site indicates a large uncertainty in the position of the H atom; in particular, the atom may be located at the center of any of the four neighboring T sites. These facts suggest that such intersite migrations are classically forbidden and dominated by deep tunneling events. Thus, these migrations can serve as fast diffusion pathways. It is interesting to note that in contrast to other metal-hydrogen systems, in Fe-H systems, a quantum description is important even at ambient temperatures.

IV. CONCLUSIONS

Our path-integral approach along with an *ab initio*–based bare potential model permits a coherent description of the temperature dependence of H diffusivity in α-Fe over a wide temperature range of 100 to 1000 K. In particular, the D values below 500 K are found to exhibit a clear non-Arrhenius behavior, which arises from the transition from classical to quantum behavior. The results reveal that quantum effects play a crucial role in the process of H migration even at ambient temperatures; quantum tunneling not only results in a significant decrease in the height of the diffusion barrier but also changes the diffusion pathway. It is important to note that of all quantum mechanical effects of interest, we focused on the *nuclear* quantum effects in the present analysis. The analysis including the effects of spin fluctuations on H diffusion would bring further insight especially with increasing temperature; however, it is beyond the scope of this paper and will be the subject of the future work. To this end, our approach can provide a general description of the quantum dynamics of H and, in certain cases, light elements (such as H, He, or Li and their isotopes) in materials over wide temperature range. This would contribute to further development of light-element-based technologies: H storage,[1,2] nuclear fission and fusion materials,[2] Li batteries,[32] etc.

ACKNOWLEDGMENTS

The authors would like to thank M. Itakura for useful discussions. This study was partially supported by Grants-in-Aid for Young Scientists (B), No. 21760077, Scientific Research (B), No. 20360055, Scientific Research on Innovative Area, "Bulk Nanostructured Metals," No. 22102003, and Challenging Exploratory Research, No. 22656030.

*kimizuka@me.es.osaka-u.ac.jp

[1] L. Schlapbach and A. Zuttel, Nature (London) **414**, 353 (2001).
[2] M. I. Hoffert *et al.*, Science **298**, 981 (2002).
[3] H. Wipf, in *Hydrogen in Metals III: Properties and Applications*, edited by H. Wipf (Springer-Verlag, Berlin, 1997), p. 51.
[4] J. Völkl and G. Alefeld, in *Hydrogen in Metals I: Basic Properties*, edited by G. Alefeld and J. Völkl (Springer-Verlag, Berlin, 1978), p. 321.
[5] K. Kiuchi and R. B. McLellan, Acta Metall. **31**, 961 (1983).
[6] Y. Tateyama and T. Ohno, Phys. Rev. B **67**, 174105 (2003).
[7] D. E. Jiang and E. A. Carter, Phys. Rev. B **70**, 064102 (2004).
[8] J. Sanchez, J. Fullea, C. Andrade, and P. L. de Andres, Phys. Rev. B **78**, 014113 (2008).
[9] M. Wen, X.-J. Xu, S. Fukuyama, and K. Yokogawa, J. Mater. Res. **16**, 3496 (2001).
[10] B.-J. Lee and J.-W. Jang, Acta Mater. **55**, 6779 (2007).
[11] A. Ramasubramaniam, M. Itakura, and E. A. Carter, Phys. Rev. B **79**, 174101 (2009).
[12] H. Kimizuka, H. Mori, H. Ushida, and S. Ogata, J. Jpn. Inst. Met. **73**, 571 (2009).
[13] M. I. Mendelev, S. Han, D. J. Srolovitz, G. J. Ackland, D. Y. Sun, and M. Asta, Philos. Mag. **83**, 3977 (2003).
[14] Here, the same parameters as those in potential 2 (in Ref. 13) were employed, but the sign of the parameter a_7^{φ} was changed from positive to negative.
[15] J. E. Angelo, N. R. Moody, and M. I. Baskes, Modell. Simul. Mater. Sci. Eng. **3**, 289 (1995).
[16] M. I. Baskes, X. Sha, J. E. Angelo, and N. R. Moody, Modell. Simul. Mater. Sci. Eng. **5**, 651 (1997).
[17] H. Jónsson, G. Mills, and K. W. Jacobsen, in *Classical and Quantum Dynamics in Condensed Phase Simulations*, edited by B. J. Berne, G. Ciccotti, and D. F. Coker (World Scientific, Singapore, 1998), p. 385.
[18] J. Cao and G. A. Voth, J. Chem. Phys. **99**, 10070 (1993); **101**, 6168 (1994).
[19] K. Kinugawa, P. B. Moore, and M. L. Klein, J. Chem. Phys. **106**, 1154 (1997).
[20] R. P. Feynman and A. R. Hibbs, *Quantum Mechanics and Path Integrals* (McGraw-Hill, New York, 1965).
[21] S. Nosé, Mol. Phys. **52**, 255 (1984).
[22] W. G. Hoover, Phys. Rev. A **31**, 1695 (1985).
[23] D. J. Tobias, G. J. Martyna, and M. L. Klein, J. Phys. Chem. **97**, 12959 (1993).
[24] G. J. Martyna, M. E. Tuckerman, D. J. Tobias, and M. L. Klein, Mol. Phys. **87**, 1117 (1996).

[25]W. L. Bryan and B. F. Dodge, AIChE J. **9**, 223 (1963).
[26]J. L. Dillard, C. R. Seances Acad. Sci. Ser. C **270**, 669 (1970).
[27]Th. Heumann and E. Domke, Ber. Bunsen Phys. Chem. **76**, 825 (1972).
[28]M. Nagano, Y. Hayashi, N. Ohtani, M. Isshiki, and K. Igaki, Scripta Metall. **16**, 973 (1982).
[29]Y. Hayashi, H. Hagi, and A. Tahara, Z. Phys. Chem. (Neue Folge) **164**, 815 (1989).
[30]H. Hagi, Mater. Trans. JIM **35**, 112 (1994).
[31]M. J. Gillan, Phys. Rev. Lett. **58**, 563 (1987).
[32]C. K. Chan, H. Peng, G. Liu, K. McIlwrath, X. F. Zhang, R. A. Huggins, and Y. Cui, Nature Nanotech. **3**, 31 (2008).